

In-vivo photoacoustic microscopy of nanoshell extravasation from solid tumor vasculature

Meng-Lin Li,^a James Chunjay Wang,^b Jon A. Schwartz,^b Kelly L. Gill-Sharp,^b George Stoica,^c and Lihong V. Wang^{d,*}

^aNational Tsing Hua University, Department of Electrical Engineering, Hsinchu, 30013, Taiwan

^bNanospectra Biosciences, Inc., Houston, Texas, 77054

^cTexas A&M University, Department of Veterinary Pathobiology, 5547 TAMU College Station, Texas 77843-5547

^dWashington University in St. Louis, Department of Biomedical Engineering, Optical Imaging Laboratory, St. Louis, Missouri 63130-4899

Abstract. In this study, high resolution backward-mode photoacoustic microscopy (PAM) is used to noninvasively image progressive extravasation and accumulation of nanoshells within a solid tumor *in vivo*. PAM takes advantage of the strong near-infrared absorption of nanoshells and their extravasation tendency from leaky tumor vasculatures for imaging. Subcutaneous tumors are grown on immunocompetent BALB/c mice. Polyethylene glycol (PEGylated) nanoshells with a peak optical absorption at ~800 nm are intravenously administered. With an 800-nm laser source, a prescan prior to nanoshell injection is taken to determine the background that is free of nanoshell accumulation. After injection, the 3-D nanoshell distribution at the tumor foci is monitored by PAM for 6 h. Experimental results show that accumulated nanoshells delineate the tumor position. Nanoshell accumulation is heterogeneous in tumors: more concentrated within the tumor cortex and largely absent from the tumor core. Because nanoshells have been recently demonstrated to enhance thermal therapy of subcutaneous tumors, we anticipate that PAM will be an important aid before, during, and after nanoshell thermal therapy. © 2009 Society of Photo-Optical Instrumentation Engineers. [DOI: 10.1117/1.3081556]

Keywords: photoacoustic microscopy; nanoshell extravasation; enhanced permeability and retention effect.

Paper 08385LR received Oct. 27, 2008; revised manuscript received Dec. 25, 2008; accepted for publication Jan. 3, 2009; published online Feb. 24, 2009.

Photoacoustic imaging is an emerging noninvasive imaging modality and has been shown to be a promising tool for visualizing tissue structures and functions by means of laser-induced ultrasound.^{1,2} Structures with high optical absorption,

such as blood vessels in the visible spectral region, can be imaged with ultrasound resolution, which is not limited by the strong optical scattering in biological tissues. Recently, an *in-vivo* backward-mode confocal photoacoustic microscope (PAM) with dark-field illumination was invented to image microvasculatures in the skin.³⁻⁵ This system offers high lateral resolution (45 μm at the focal point), high axial resolution (~15 μm), and is capable of imaging optical absorption contrast as deeply as 3 mm. It shows great potential for applications in dermatology and related cancer research.

Contrast-agent-enhanced optical imaging techniques possess high sensitivity and specificity. In this study, we use gold nanoshells (AuroShell™ Particles, Nanospectra Biosciences, Incorporated, Houston, Texas) as a contrast agent for photoacoustic microscopy of tumors. Gold nanoshells have been applied to photothermal therapy of subcutaneous murine tumors⁶ and have also been used as a contrast agent for *in-vivo* brain imaging with photoacoustic tomography, enhancing contrast of cortex vessels in rat brain.⁷ Gold nanoshells are a new type of optically tunable nanoparticles, composed of silica cores (~116 nm in diameter) coated with an ultrathin gold shell (~14 nm).⁸ By adjusting the core size relative to the thickness of the gold shell, the optical properties of nanoshells can be varied across a broad range of the electromagnetic spectrum that spans the visible and infrared regions. In our cancer applications, gold nanoshells are designed to absorb light at near-infrared (NIR) wavelengths. The peak optical absorption of nanoshells in this study is at a wavelength of ~800 nm that corresponds to optimal penetration into scattering biological tissues, and is the isosbestic point of the molar extinction spectra of oxy- and deoxyhemoglobin, thus reducing the effect of blood oxygenation variations on photoacoustic signals.⁷ Nanoshells tend to preferentially extravasate from leaky tumor vasculatures and accumulate in tumors—a preferential, size- and shape-dependent accumulation—via the enhanced permeability and retention effect due to their nanoscale size (i.e., passive targeting).⁹⁻¹¹ The end result of nanoshell accumulation is greatly enhanced NIR optical absorption contrast in the vicinity of tumor vasculatures. In addition, the gold nanoshells used in this study were coated with 5-kD polyethylene glycol (PEG) to increase their circulation time in the blood stream. The PEGylated nanoshells were measured to have a half-life of ~3.7 h in the blood stream of immunocompetent BALB/c mice.⁷

In this study, the PAM was used to noninvasively image the progressive extravasation of gold nanoshells through solid tumor vasculature *in vivo*. High resolution and high contrast 3-D gold nanoshell distribution at the solid tumor foci was imaged for 6 h. This technology allows us to monitor the dynamics of nanoshells in the solid tumor without any invasive biological modification such as the use of a dorsal skin-fold window chamber.⁹

Figure 1 shows the experimental setup of a photoacoustic microscope for *in-vivo* imaging of nanoshell extravasation in solid tumors. A tunable Ti:sapphire laser (LT-2211A, Lotis TII) pumped by a Nd:YAG laser (LS-2137/2, Lotis TII) was employed to provide pulses with a pulse width of 15 ns, a pulse repetition rate of 10 Hz, and a wavelength of 800 nm, the peak optical absorption wavelength of the nanoshells used

*Address all correspondence to: Lihong V. Wang, Department of Biomedical Engineering, Washington University in St. Louis, Campus Box 1097, One Brookings Drive, St. Louis, MO 63130-4899. Tel: 314-935-6152; Fax: 314-935-7448; Email: lhwang@biomed.wustl.edu.

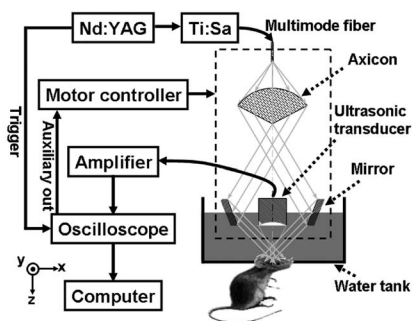


Fig. 1 Schematic of the photoacoustic microscope for nanoshell imaging: Ti:Sa, Ti:sapphire.

in this study. The laser energy was delivered by a multimode fiber with a 0.6 mm diameter. The fiber tip was coaxially positioned on a 3-D precision mechanical scanner. An axicon and a mirror were used to form dark-field illumination and make the light confocal with a 50-MHz focused ultrasonic transducer (V214-BC-RM, Panametrics), whose fractional bandwidth is 70%. The incident energy density on the sample surface was controlled to $<2 \text{ mJ/cm}^2$, which is well within the ANSI standards. A homemade concave lens provided this transducer with a numerical aperture of 0.44 and a focal length of 6.7 mm, offering a lateral resolution of $45 \mu\text{m}$ and an axial resolution of $15 \mu\text{m}$. The lens was ground from the permanent fused-silica delay line attached to the transducer. The transducer was immersed in a water tank, which had a hole at the bottom sealed with a piece of polyethylene membrane. The imaged part of the animal (e.g., the head of the mouse) was coated with a thin layer of ultrasonic gel and then placed below the membrane. The photoacoustic signals received by the ultrasonic transducer were amplified and recorded by a digital oscilloscope (TDS 5034B, Tektronix) at a 250-MHz sampling rate. Note that the photoacoustic images shown were taken without signal averaging, and the brightness of the images represents the amplitude of the detected photoacoustic signals.

Immunocompetent BALB/c mice weighing about 20 g were used for the *in-vivo* experiments. All of the experimental animal procedures were approved by the University Laboratory Animal Care Committee of Texas A&M University. The mice were inoculated with CT26.wt murine colon carcinoma cells subcutaneously on the heads. The mouse head was a good model for long-term immobilization required in our experiments. Imaging was performed 7 days after tumor inoculation and under isoflurane gas anesthesia with a dose of 1% in pure oxygen at a 1-L/min flow rate. We maintained the temperature of the imaged tumor region at 39°C by controlling the temperature of the water in the tank.^{9,12} The body temperature of the animal was maintained by using a water heating pad and a lamp; the pulse rate and arterial blood oxygenation were monitored using a pulse oximeter (model 8600, Nonin Medical, Incorporated) clamped on the back paw. A prescan prior to nanoshell administration was performed to determine the background signal. PEGylated nanoshells with a peak optical absorption at $\sim 800 \text{ nm}$ were then intravenously administered. The nanoshell dose was about 1.4×10^9 -nanoshells/g body weight (~ 1.8

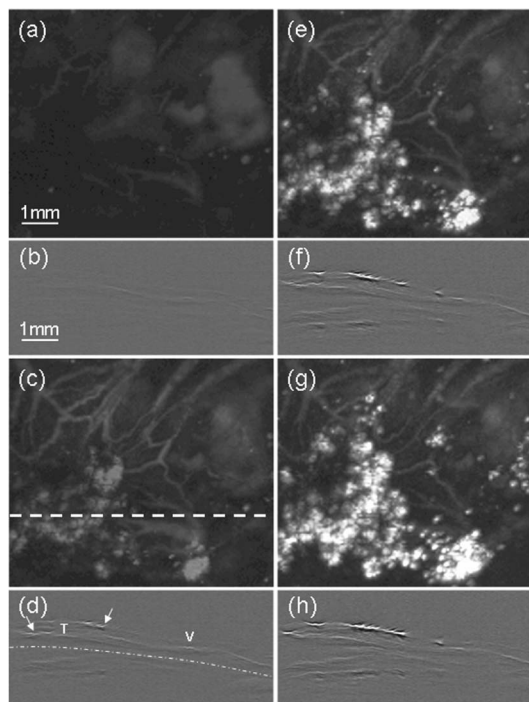


Fig. 2 *In-vivo* noninvasive photoacoustic images of nanoshell extravasation from solid tumor vasculature. (a), (c), (e), and (g) show *in-vivo* maximum-amplitude-projected (MAP) images acquired prior to nanoshell administration and at 1.4, 3, and 5.8 h postnanoshell administration, respectively. The horizontal and vertical axes indicate the scanning position of the acoustic transducer. (b), (d), (f), and (h) show *in-vivo* B-scan images that correspond to the scanning position indicated by the white dashed line in (c) and are acquired before and at 1.4, 3, and 5.8 h after nanoshell injection, respectively. The vertical axis is the imaging depth and the horizontal axis is the lateral scanning position. In (d), the dash-dotted line is the depth of skull; T is tumor; V is vessel; and arrow is nanoshell.

$\times 10^{10}$ nanoshells/ml blood). At this concentration, the absorption coefficient due to nanoshells is $\sim 7 \text{ cm}^{-1}$ at 800 nm. In comparison, the absorption coefficient of whole blood at 800 nm is $\sim 4 \text{ cm}^{-1}$. After injection, the 3-D nanoshell distribution at the tumor foci was monitored by PAM for 6 h. After imaging, the mice were sacrificed using pentobarbital overdose (120 mg/kg, IP). The imaged tumor and surrounding tissue were excised and stained with hematoxylin and eosin (HE) for histology.

PAM measurements illustrate the passive uptake of nanoshells at the inoculated tumor foci. Figures 2(a), 2(c), 2(e), and 2(g) are maximum-amplitude-projected (MAP) images taken prior to and at 1.4, 3, and 5.8 h postnanoshell injection, respectively. In the MAP images, the maximum value of the photoacoustic signal of each A-line along the depth direction versus the 2-D transducer position is plotted. The images are shown on the same grayscale. It is shown in Fig. 2(a) that without nanoshell injection, the intrinsic blood absorption contrast is relatively low. The nanoshells increase the signal amplitudes from blood vessels by a factor of 2, thus, enhancing the contrast of blood vessels. With the help of nanoshells, Figs. 2(c), 2(e), and 2(g) show the feeding vessels and accumulated nanoshells at tumor foci well. The nanoshell accumulation gradually delineates the tumor contour and po-

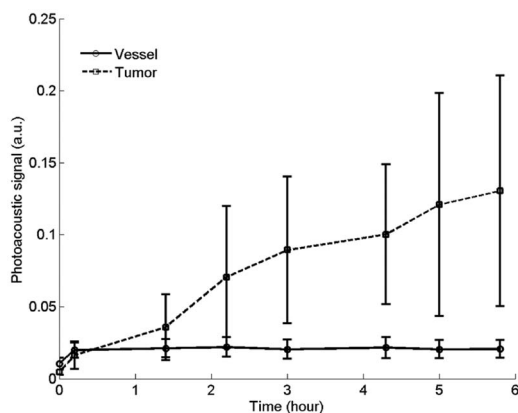


Fig. 3 Averaged photoacoustic signals as a function of time. Line with circles: vessel regions; dashed line with squares: tumor foci. 0 h represents “prior to nanoshell injection.” Error bar represents plus and minus one standard deviation.

sition, which cannot be visualized without nanoshells.

Figures 2(b), 2(d), 2(f), and 2(h) show the B-scan images, of which the scanning position corresponds to the white dashed line in Fig. 2(c), and are acquired before and at 1.4, 3, and 5.8 h after nanoshell injection, respectively. The images are shown on the same grayscale. The brightness represents the photoacoustic pressure amplitude detected by the transducer. In the B-scan images, the vertical axis is the depth and the horizontal axis is the lateral scanning position. In Fig. 2(d), the character “T” marks the tumor core position; the character “V” indicates the depth of one feeding vessel of the tumor. The bright spots in Figs. 2(d), 2(f), and 2(h), at the positions indicated by the arrows in Fig. 2(d), are the photoacoustic signals from accumulated nanoshells. These B-scan images reveal the depth information where nanoshells accumulate, which also indicate that the nanoshells distribute mainly around the tumor cortex. Similar results were observed on several mice. Most signals shown below the dashed-dotted line (i.e., skull position) in Fig. 2(d) are skull-reflected photoacoustic signals.

Absence of nanoshells within the tumor core is observed in Figs. 2(d), 2(f), and 2(h). We show that nanoshell accumulation is heterogeneous in tumors: largely absent from the tumor core and more concentrated within the tumor cortex, as shown in literature.^{12,13} The difficulties in delivery of nanoparticles within tumor cores are possibly caused by both the high interstitial pressure and the avascularity of necrotic tumor cores.¹²⁻¹⁴

Time-dependent variation of absorption in the vessels and tumor foci attributable to the injected nanoshells can be observed via changes in photoacoustic signals. Figure 3 shows the averaged photoacoustic signals at vessels and tumor foci in the MAP images of Fig. 2, respectively, as a function of time. The results show the clearance and accumulation profiles of the nanoshells in vessels and tumor regions, respectively: nanoshells in the vessels are gradually cleared out by the reticuloendothelial system of the mouse, and those in the tumor foci are progressively taken up, owing to poor lymphatic drainage of the tumor (i.e., the enhanced permeability and retention effect). At 5.8 h after nanoshell injection, the contrast ratio of the tumor foci to the vessels is ~6.5.

In summary, by employing PAM, we successfully image extravasation of gold nanoshells from solid tumor vasculature *in vivo*. Using exogenous contrast from nanoshells, image contrast is significantly enhanced at 800 nm, whether it is vessels or tumor foci. It is also found that nanoshell accumulation is heterogeneous in tumors. Because gold nanoshells have been recently applied to photothermal therapy for subcutaneous tumors, we anticipate that the integration of PAM into gold-nanoshell-based photothermal therapy to characterize and monitor the accumulation of gold nanoshells in solid tumors would be an invaluable aid.^{6,7} In addition, by using bioconjugated gold nanoshells that target specific molecular signatures of disease, the technique presented here (i.e., PAM plus nanoshells) can potentially enable molecular imaging.¹⁵

Acknowledgments

We are grateful to Gina Lungu and Ovidiu Craciun for their assistance with cell culture and veterinary procedure, and to Jung-Taek Oh, Hao F. Zhang, and Konstantin Maslov for their technical advice and prior system development. This project is sponsored in part by the National Institutes of Health grants R01 EB000712 and R01 NS46214, and in part by the Advanced Technology Program at NIST, cooperative agreement 70NANB4H3040.

References

1. M. Xu and L. V. Wang, “Photoacoustic imaging in biomedicine,” *Rev. Sci. Instrum.* **77**, 041101-1–041101-22 (2006).
2. L. V. Wang, “Ultrasound-mediated biophotonic imaging: a review of acousto-optical tomography and photoacoustic tomography,” *Dis. Markers* **19**, 123–138 (2004).
3. K. Maslov, G. Stoica, and L. V. Wang, “*In vivo* dark-field reflection-mode photoacoustic microscopy,” *Opt. Lett.* **30**, 625–627 (2005).
4. M.-L. Li, H. F. Zhang, K. Maslov, G. Stoica, and L. V. Wang, “Improved *in vivo* photoacoustic microscopy based on a virtual-detector concept,” *Opt. Lett.* **31**, 474–476 (2006).
5. H. F. Zhang, K. Maslov, G. Stoica, and L. V. Wang, “Functional photoacoustic microscopy for high resolution and noninvasive *in vivo* imaging,” *Nat. Biotechnol.* **24**, 848–851 (2006).
6. D. P. O’Neal, L. R. Hirsch, N. J. Halas, J. D. Payne, and J. L. West, “Photo-thermal tumor ablation in mice using near infrared-absorbing nanoparticles,” *Cancer Lett.* **209**, 171–176 (2004).
7. Y. Wang, X. Xie, X. Wang, G. Ku, K. L. Gill, D. P. O’Neal, G. Stoica, and L. V. Wang, “Photoacoustic tomography of a nanoshell contrast agent in the *in vivo* rat brain,” *Nano Lett.* **4**, 1689–1692 (2004).
8. S. J. Oldenburg, J. B. Jackson, S. L. Westcott, and N. J. Halas, “Infrared extinction properties of gold nanoshells,” *Appl. Phys. Lett.* **75**, 2897–2899 (1999).
9. G. Kong, R. D. Braun, and M. W. Dewhirst, “Characterization of the effect of hyperthermia on nanoparticle extravasation from tumor vasculature,” *Cancer Res.* **61**, 3027–3032 (2001).
10. X. Gao, Y. Gui, R. M. Levenson, L. W. K. Chung, and S. Nie, “*In vivo* cancer targeting and imaging with semiconductor quantum dots,” *Nat. Biotechnol.* **22**, 969–976 (2004).
11. P. Decuzzi, R. Pasqualini, W. Arap, and M. Ferrari, “Intravascular delivery of particulate systems: does geometry really matter?,” *Pharm. Res.* **26**, 235–243 (2009).
12. P. Liu, A. Zhang, Y. Xu, and X. Xu, “Study of non-uniform micro-particulate liposome extravasation in tumour,” *Int. J. Hyperthermia* **21**, 259–270 (2005).
13. R. Jain, “Transport of molecules, particles, and cells in solid tumors,” *Annu. Rev. Biomed. Eng.* **1**, 241–263 (1999).
14. T. P. Padera, B. R. Stoll, J. B. Tooredman, D. Capen, E. di Tomaso, and R. K. Jain, “Pathology: cancer cells compress intratumour vessels,” *Nature (London)* **427**, 695 (2004).
15. C. Loo, L. Hirsch, M. H. Lee, E. Chang, J. West, N. Halas, and R. Drezek, “Gold nanoshell bioconjugates for molecular imaging in living cells,” *Opt. Lett.* **30**, 1012–1014 (2005).